

Design and Preliminary Results of a Reaction Force Series Elastic Actuator for Bionic Knee and Ankle Prostheses

Matthew E. Carney,¹ *Member, IEEE*, Tony Shu,¹ Roman Stolyarov,¹ Jean-François Duval,² Hugh Herr,¹

Abstract—We present an untethered, lower-extremity powered-prostheses designed to replicate biological kinetic and kinematic function of both human knees and ankles. An energy optimal hardware specification was found by kinematically clamping walking gait data to the dynamic model of a series elastic actuator (SEA). We searched for a minimal electrical energy configuration of motor, reduction ratio, and spring, subject to specified constraints and ultimately discretely available components. The outcome translated into a mechanical design that heavily weighted the importance of mechanical energy storage in springs. The resulting design is a moment-coupled cantilever-beam reaction-force SEA (RFSEA) that has a nominal torque rating of 85Nm, peak torque of 175Nm, 105 degree range of motion, and a hardware mass of 1.6kg.

Index Terms—robotics, prostheses, actuator, ankle, knee.

I. INTRODUCTION

A little more than a decade after the first powered ankle prosthesis, research in lower-extremity rehabilitation robotics remains limited by a lack of commercial and academic hardware platforms capable of producing biologically relevant dynamics. The commercial off the shelf powered ankle and knee systems are not able to provide biologically accurate kinetics with kinematics, nor do they enable access to the underlying control systems [1], [2]. To improve upon the commercial options, a growing handful of academic research groups around the world have been building individualized platforms for study. Most of these academic platforms have mostly remained within their own labs requiring each lab to build its own hardware. This paper describes the mechanical design of an autonomous, untethered, wearable, series elastic actuator topology that aims to achieve biologically relevant kinetics and kinematics of both a human knee and ankle, while remaining within the mass bounds of human equivalent leg segments and reduced the hardware complexity.

The first powered ankle, published by Au, Weber, Herr, used a series elastic actuator (SEA) [3] configured with a parallel spring to improve torque bandwidth in the transition from controlled dorsiflexion to powered-push-off. Au *et al.*

Manuscript received Month, Year.

Financial support: this work was supported in part by the MIT Media Lab Consortia, the U.S. Army Medical Research and Materiel Command (W81XWH-14-C-0111) and the Defense Advanced Research Projects Agency (W911NF-17-2-0043).

¹MIT Center for Extreme Bionics and MIT Media Lab - Biomechanics Group, Massachusetts Institute of Technology, Cambridge, MA 02139 USA. e-mail: mcarney@mit.edu.

²Dephy, Inc., Maynard, MA 01754 USA.

showed that their actuator’s ability to contribute energy during powered push-off improved the metabolic cost of walking [4]. Since then numerous actuators have been designed following a similar actuator topology [5]–[9]. Many of these designs have focused around flat, level-ground walking, where primary kinetic behavior occurs as a large power maneuver during powered plantar flexion. Commercial devices such as the BiOM [10] even limit joint range to zero dorsiflexion in order to reduce electric energy expenditure. To improve control bandwidth and electrical energetics parallel springs are frequently used, at a cost of range of motion and terrain adaptability.

Though well designed for flat ground, and self-selected walking speed, these systems quickly hit kinematic limits at higher walking velocities and varied terrain. At higher walking speed, stride length and joint angle extension increase [11]. Mean data from nine subjects walking at 0.75m/s to 2.0m/s shows dorsiflexion angle increases from 8.3 to 19.3 degrees though plantar flexion angle changes from 19.8 – 14.9 degrees. These range of motion limitations are compounded when encountering sloped surfaces or stairs. During stair descent [12] found a 21 degree mean dorsiflexion angle during stance and 40 degree mean plantar flexion angle in swing phase. Since the ADA compliant power wheelchair ramp slope specification declares a maximum 7.1 degree inclination, fast walking up such a ramp eliminates or limits proper kinematic function in all the ankles described except for the Vanderbilt legs even before considering user specific orientation preferences.

In this study we present the mechanical design of TF8¹, an actuator that aims to achieve biological kinetics and kinematics equivalent to that of a human knee and ankle while remaining within the mass constraints of equivalent leg segments. We simulate the energetic consequences of a unidirectional parallel spring, and series spring stiffness when coupled to a large-gap-radius motor tracking kinematic trajectories, following a process described in an accompanying paper [13]. We then present the optimization procedures used to design the mechanical linkage geometry, and series springs implemented in the design. Finally, we present the the final design and preliminary results of below-knee, level-ground walking with the TF8 ankle actuator.

¹The TF8 name comes from being the eighth major design iteration of what was originally to be a powered knee prosthesis for transfemoral (above knee amputee) subjects.



Fig. 1. The TF8 Actuator is designed to operate as either a knee or ankle powered prosthesis – shown here it is configured as an ankle prosthesis.

II. METHODS

We aim to design and build an autonomous lower-extremity powered prostheses capable of providing biologically equivalent kinetic and kinematic trajectories while minimizing electric energy consumption. The resulting design should be equal to or lighter weight than an equivalent normative biological limb segment, enable physical tasks beyond level-ground walking such as sit-to-stand, inclinations, stairs, jogging, or fall recovery, and if possible be capable of functioning as both a knee and an ankle prosthesis.

A. Design Specification

To determine the design specification for range of motion, torque, power, and system bandwidth, we normalized and scaled by body mass a total of 1005 unique gait cycles of walking data from nine able-bodied subjects collated from [14]. Details of this design process can be found in our paper [13]. We set the performance target based on a 90kg user walking at a near jogging pace of 2.0m/s. The design goal to enable performance of daily tasks and walking on uneven terrains requires a larger range of motion than that defined only by walking [15]. The performance objectives we aimed to achieve with the design of this actuator are summarized in the design parameter specification Table I.

We derived the mass allowance of the device by evaluating the mass of equivalent leg segments. The mass of a human calf and foot segment is 5.82% of body mass, while the mean calf mass is 4.35% and the mean foot segment mass is 1.47% [16]. We assume a reasonable assumption of the mass accommodation of a prosthetic ankle-foot used for this design is the mass of a foot and one third of the calf mass, or 2.9% of body mass. For a 90kg subject this allows 5.2kg for a combined above-knee and below-knee prosthesis, and for an individual below-knee prosthesis 2.6kg was an equivalent

TABLE I
ACTUATOR DESIGN SPECIFICATION

2m/s	Ankle	Knee	Target	Units
Range of Motion ¹	19-0-19	70	45-0-65	Deg
Velocity	6.0	8.6	7	rad/s
Max Torque	160	118	175	Nm
Max Power	552	313	550	W
Bandwidth Magnitude	82	73	82	Nm
Bandwidth Frequency	4.8	6.0	6.0	Hz
Segment Mass	2.6	2.6	2.0	kg

¹ Range of motion as shown: *dorsiflexion - neutral - plantar flexion*.

mass allowance. Despite these allowances, it should be noted: prostheses should generally be as light as possible due to limitations with prosthesis suspension.

B. Mechanical Design

Following a process similar to [17]–[19] we evaluated the performance of a series elastic actuator kinematically clamped to biological gait data while searching for drivetrain component specifications for the spring, motor and drivetrain that meet the search objective. Our process is outlined in [13], where we also evaluated the electric energetic consequences of varied gear reduction, spring stiffness and the contributions of unidirectional parallel springs for walking on level-ground and stairs. The parallel element has been used to improve control bandwidth and improve energetics in level-ground walking [4], [6], [20]. However, the parallel element also increases system complexity and mass, while the energetic improvements were not deemed substantial enough to be included in this design.

1) *Optimization*: We applied a gradient descent optimization procedure with non-linear constraints to a model of the mechanical and electrical systems dynamics to find the main parameters of interest: motor voltage and current requirements, transmission ratio, series stiffness (K_s), parallel stiffness (K_p), and parallel spring engagement point (X_{p0}). Mean torque, velocity and angle trajectories aggregated from [14] were mass normalized, scaled and kinematically clamped to the dynamic equations for a series elastic actuator. To identify the necessary component parameters for powered prosthesis joint actuators, we used an optimization process similar to [17], [18] and defined in [13]. We set the search objective to minimize the electric Cost of Transport (COT) for a gait cycle. We aggregated the results and sorted them by minimum electric energy consumption. In narrowing the design architecture we chose to use a linear ballscrew and linkage drive train. We then implemented secondary tiered optimization searches to identify an energy optimal joint linkage geometry and a mass optimized spring.

2) *Linkage Geometry*: Joint torque is generated by a linear actuator that acts on a moment arm about the joint axis. The linear actuator is composed of a ballscrew integrated into a motor rotor. The rotation of the screw is limited by a push-rod end affixed to one end that pivots around an orthogonal axis located a projected distance r from joint axis. We used a gradient descent search to tune the linkage geometry to

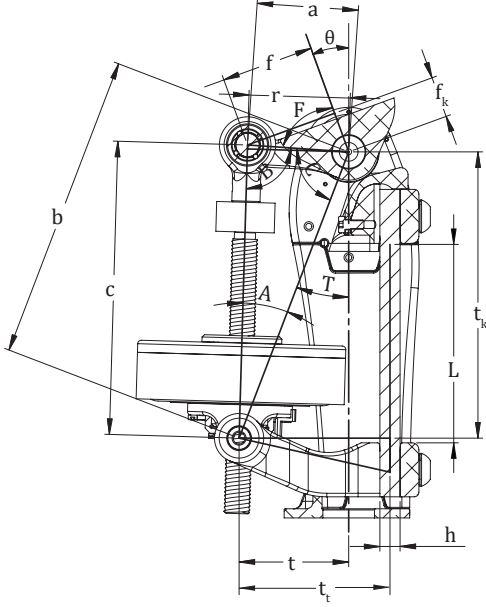


Fig. 2. Linkage geometry labels. The optimization procedure searched for the t, t_k, f, f_k, L geometry parameters. The objective was finding moment arm geometry with the most efficient configuration of the power stroke as specified by the load trajectory and actuator dynamics.

match the power-stroke of an ankle gait cycle by setting the search objective to minimize COT. The linkage parameters we searched for f, f_k, t, t_k are defined in Fig. 2.

Applying the law of cosines we can define the screw length and moment arm as:

$$a = \sqrt{f^2 + f_k^2} \quad (1)$$

$$b = \sqrt{t^2 + t_k^2} \quad (2)$$

$$T_\theta = \arctan\left(\frac{t}{t_k}\right) \quad (3)$$

$$F_\theta = \arctan\left(\frac{f}{f_k}\right) \quad (4)$$

$$C_\theta = \pi - \theta_l - (T + F) \quad (5)$$

$$c = \sqrt{a^2 + b^2 - 2 \cdot a \cdot b \cdot \cos(C_\theta)} \quad (6)$$

$$A_\theta = \arccos\left(\frac{a^2 - (c^2 + b^2)}{-2bc}\right) \quad (7)$$

$$r = b \cdot \sin(A_\theta) = b \cdot \sqrt{1 - \left(\frac{a^2 - (c^2 + b^2)}{-2bc}\right)^2} \quad (8)$$

where, r is projected distance of the screw force along C , about the joint pivot defined at angle θ .

3) *Elastic Elements*: To achieve the component specification for an elastic element we optimized a cantilever beam as a spring to meet the energy storage requirement while minimizing mass and subject to geometric constraints.

The cyclical motion of gait is well suited to leverage the energy storage and power delivery capacity of springs [21]. The goal of the series elastic element design is to maximize energy storage in the spring while also maximizing sys-

TABLE II
STRAIN ENERGY DENSITY OF MATERIALS

Material	E	G	σ_f^1	ρ	$\frac{\Delta U}{\Delta m}$
	[GPa]	[GPa]	[MPa]	$[\frac{g}{cm^3}]$	$[\frac{J}{kg}]$
GC-70-UCL ²	137	52.7	836	1.55	1646
GC-67-UB ²	40	15.4	381	1.88	961
Maraging Steel	200	76.9	1208	8.08	451
Ti-6Al-4V	114	42.2	585	4.43	339
Ultramid PA6/66	1.4	1.4	32	1.1	332
17-7 Ph CH900	204	78.5	660	7.8	137
7075-T6	72	27	172	2.8	73

¹ Allowable fatigue endurance limit is assumed $0.5\sigma_u$ for steel, $0.4\sigma_u$ for composites and plastics, and $0.3\sigma_u$ for aluminum alloys.

² Unidirectional composite fibers aligned in 0° [23].

tem control bandwidth – two opposing objectives. Increasing spring stiffness improves natural frequency, but reduces the amount of energy that can be stored for a given loading condition, and puts greater precision requirements on encoder based force sensing. Reduced spring stiffness improves energy storage but also requires the motor to travel greater distance to reverse direction at high load.

Compressing a spring requires work, a force applied over a distance. This work deforms a volume of material by twisting, bending or pushing to change its shape. This deformation of a volume of material is strain, and the energy embodied in strain increases until material structural bonds begin to fail.

Spring design seeks to find materials that maximize strain and stress while also fitting geometric requirements. To fully utilize material volume the goal is to make an equal distribution of strain throughout the entire volume of material while it is stressed just to the yield limit. To compare candidate materials we look to the average strain energy density for uniaxial deformation, in $[\frac{J}{kg}]$ [22]:

$$\frac{\Delta U}{\Delta m} = \frac{1}{2} \frac{\sigma^2}{E\rho} \quad (9)$$

where, ϵ is strain, σ is stress, E is Young's Modulus, ΔV is change in volume.

A selection of potential spring materials are shown in Table II. Polymers such as nylon or polyurethanes perform well, though their internal viscoelastic damping results in hysteresis and their strain-rate dependent modulus of elasticity is not favorable for the this analysis [24]. Non-isotropic materials such as composites can be tuned to maximize mass utilization with fiber alignment when stress orientation is considered along with geometric conditions.

The series elastic element in TF8 is a cantilever beam that primarily undergoes moment bending when the reaction force of the motor and screw is applied by way of a moment arm clamped to the beam generating a force-couple. The energy stored in the spring is primarily due to bending and axial strains, though shear strains due to screw askew orientation also apply:

$$U_{bend} = \frac{M^2 L}{2EI} = \frac{L(P_x t + LP_y)^2}{2EI} \quad (10)$$

$$U_{axial} = \frac{P_x^2 L}{2AE} \quad (11)$$

$$U_{shear} = \frac{P_y^2 h}{2AG} \quad (12)$$

$$U_{total} = U_{bend} + U_{axial} + U_{shear} \quad (13)$$

where, P_x , P_y are the screw force F_s , contributions defined as:

$$P_x = F_s \cos \theta_p \quad (14)$$

$$P_y = F_s \sin \theta_p \quad (15)$$

where,

$$\theta_p = \frac{F_s}{K_x t} \quad (16)$$

, K_s is linear spring stiffness, and t is the moment arm length as described in Fig. 2 and our component specifications.

We numerically solve for spring geometry L , h , b . Specifying the desired stiffness K_s , and stored energy (13) defined by our component specifications, we then search for minimum mass configurations that satisfy our allowable design constraints for beam height, width, and length. The beam height is constructed from:

$$h = \sqrt[6]{\frac{(P_x t + P_y L)}{b \cdot \sigma_f}} \quad (17)$$

where, b and L are beam width and length, respectively, and σ_f is the allowable fatigue limit of the material.

4) *Spring Characterization*: To measure joint torque by way of spring deflection we characterize the total structural loop stiffness. The angular stiffness of the cantilever beam is combined with the geometry of the actuator to determine the linear stiffness of the spring. Real screw force was measured with an in-line 4.5 kN load cell (Futek LCM300 [25]) in order to verify the encoder based force measurements using 19. Utilizing the Euler-Bernoulli (E-B) bending beam approximation of a beam with a pure moment we define the angular stiffness as:

$$K_\theta = \frac{EI}{L} \eta_k, \quad (18)$$

where, we include η_k as a fitting factor to accommodate additional elasticity in the structure not captured by the beam equation. The small angle approximation applies to the expected deflections in our system, allowing simplification of the force measurement based on the linear displacement of the screw, and effective linear stiffness of the actuator, K_x :

$$F_s = \Delta K_x, \quad (19)$$

$$\Delta = X_m - X_l(\theta) \quad (20)$$

$$K_x = \frac{K_\theta}{t^2}, \quad (21)$$

Here, we define Δ as the displacement of the screw measured in the difference between motor position X_m and expected motor position due to output joint orientation $X_l(\theta)$.

In practice we found that encoder based force sensing is highly dependent on the precision of system geometry and backlash. To calibrate our force sensing we collected joint

angle and motor angle measurements and searched for linkage geometry that found the minimal torque error through the full range of motion of the actuator.

5) *Structure*: We estimated maximum allowable structural deflections of the actuator by considering the average level-1 cross-sectional thickness and second area moment of inertia of tibial bone, as specified by Milgrom *et al.* [26]. In-vivo experiments show deflection angles of 0.5-1 degrees anterior-posterior, 1.5deg torsion and 0.5deg medial-lateral during normal walking [27]. With a modulus of elasticity of about 6GPa [28], a value close to nylon, the tibia has a measured stiffness in the anterior-posterior direction of 6Nm/mm, 3.5Nm/mm in the medial-lateral direction [29]. The parameters for tibial bone were applied with the E-B bending beam equation to determine the maximum deflection for an equivalent leg segment with a height of 180mm and a user body mass of 90kg.

C. Mechatronics and Controls

The mechatronic system is composed of a control unit that houses a mid-level controller, motor driver, battery management system, sensor inputs and communications to external peripherals. This architecture enables on-board autonomous control of a powered prosthesis with the expandability to more computationally intensive control from external devices. The control unit is a modified version of the Dephy Inc. FlexSEA system [30]. The mid-level controller is based on a STM32F427 180Mhz microprocessor. The external sensors include an absolute on-axis joint encoder (AS5048B), incremental off-axis motor encoder (RLM2), and load-cell (LCM300). Internal sensors include an inertial measurement unit, motor phase current sensor, wheat-stone bridge strain-gauge circuit, and a temperature sensor. The peripheral communications allow communication between a host computer through USB, Bluetooth and RS485 for additional master/slave FlexSEA units. Additionally, an I²C bus is used to communicate with an external electromyography (EMG) amplifier board also designed by our research group. The block diagram of this control unit is shown in Fig. 3.

1) *System Characterization*: This actuator is a reaction force series elastic actuator; the actuator free-space and high-impedance behavior differ from a traditional SEA. The primary difference is the spring is serially located in the ground-path of the motor, rather than the output path of the actuator. The lumped parameter assumption commonly utilized for a SEA is not valid for free-space motions, and in the high-impedance case motor-mass is also sprung with the rotor inertia. The performance of the high-impedance condition differs from the low-impedance moving output condition by enabling an impulse load to deflect the spring and motor without rotating the motor inertia, thus improving high-frequency inertial conditions [31], [32]. For the high-impedance condition we use the lumped model for system performance estimates:

$$\frac{F_s}{F_m} = \frac{k}{m_k s^2 + b_m s + k} \quad (22)$$

$$(23)$$

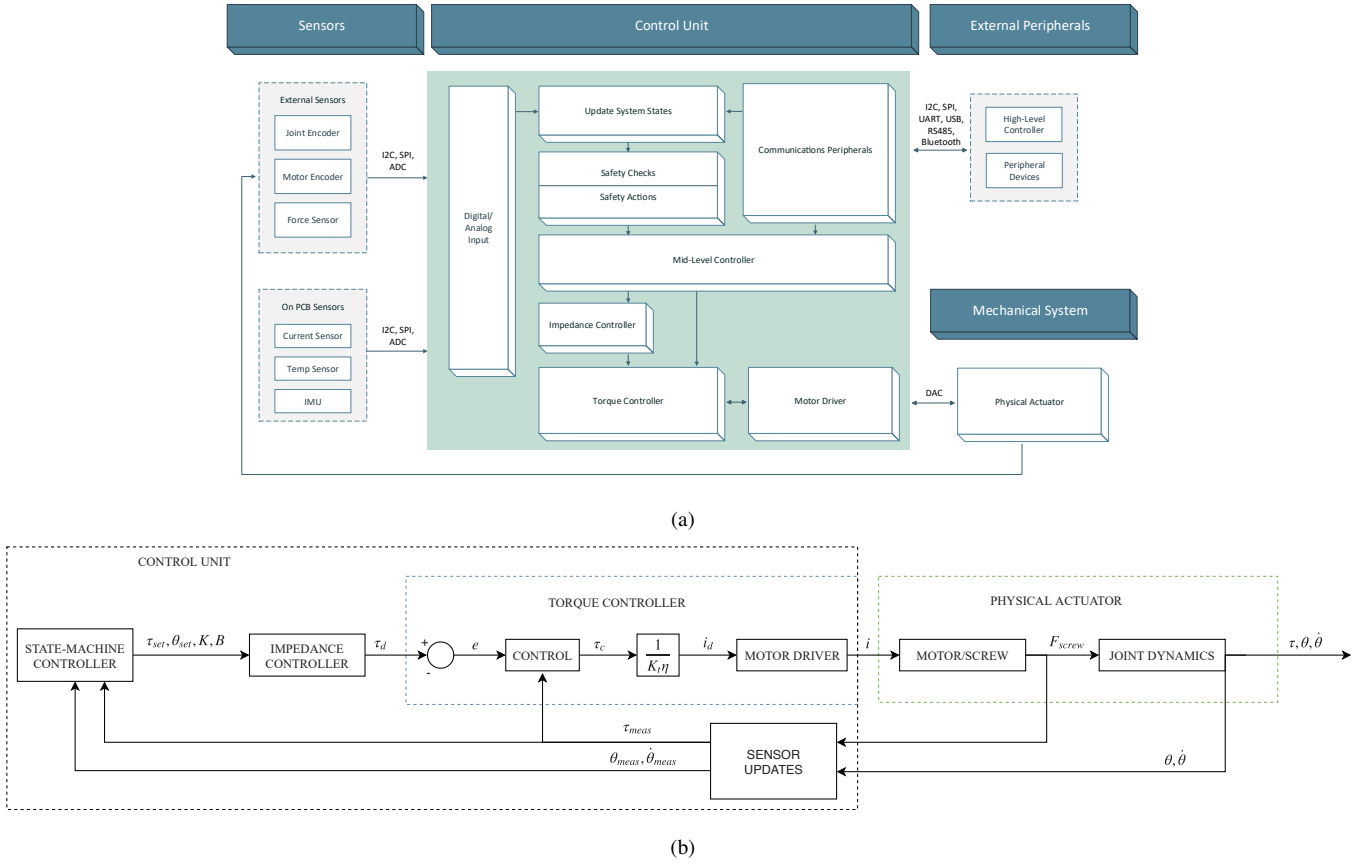


Fig. 3. (a) Mechatronic system layout. The Control Unit is based on the FlexSEA embedded system developed by Dephy, Inc. consisting of a motor driver and a STM32F427 based mid-level micro-controller that supports external peripheral devices, sensors, and common communication protocols. (b) Basic closed-loop feedback torque control diagram.

where, F_m is motor force, $m_k = m_l + N^2 J_m$, is the lumped equivalent mass, m_l is the mass of translational elements (motor and screw), J_m is rotor inertia, N^2 is the reduction ratio, and b_m is equivalent reflected damping.

To verify bench-top actuator capabilities of the TF8 actuator we drove it to its designed maximum L10 fatigue limit load rating: a maximum screw force of 4365N, an equivalent 180Nm at the output, Fig. 7.

2) *Torque Compensator*: The control block diagram is shown in Fig. 3(b). The torque compensation loop operates at 1kHz on the control unit board and requests motor current from the motor-driver board. The current controller is operating at 20kHz. The desired torque command is updated at 100 Hz by the mid-level controller.

For preliminary evaluation the torque compensator is a proportional differential (PD) controller. Controller gain tuning was done manually with the joint statically locked in position. Desired torque step inputs of 30Nm were commanded and we adjusted gains to find a system response that balanced overshoot with settling time, weighted more towards settling time. More sophisticated controls could be applied to the system that further maximize the potential of the hardware.

3) *Impedance Controller*: Joint torque is specified by the mid-level impedance controller. We then command a desired current to the motor driver to enforce at the motor. The

impedance torque command follows the form:

$$\tau_d = K_d(\theta_{des} - \theta_l) - B(\dot{\theta}_l) \quad (24)$$

where, τ_d is desired joint torque specified to the torque controller, θ_{des} is desired joint angle set point, θ_l is measured joint angle, and $\dot{\theta}_l$ is measured joint velocity. The initial impedance parameters utilized were from [33]. User testing found that these parameters were modified substantially to accommodate the different hardware response and varying user preference.

4) *Finite-State Machine*: To demonstrate TF8's ability to achieve biologically relevant kinetics and kinematics behaviors we implemented an ankle walking finite-state machine in the mid-level controller following [34]–[37]. The state transitions are shown in Fig. 4. Stiffness, damping torque thresholds, push-off toe angle, and torque ramp rate are all manually tuned to user preference during an acclimation period.

Stance is triggered by a heel-strike transition identified by an absolute torque signal greater than a set threshold. Controlled-dorsiflexion superposes a unidirectional virtual parallel spring on top of the stance impedance settings. As the subject leans into the virtual parallel spring joint torque rises until reaching a specified threshold at which point the powered plantarflexion state triggers. The joint angle set point then ramps to the next position along with a transition in virtual stiffness and damping. As the user is propelled forward and lifts their foot the torque drops below a threshold and the swing phase is

triggered. Swing phase then rapidly moves the toe position into a dorsiflexed state to provide clearance throughout swing and the controller waits for the next heel strike.

D. Preliminary Clinical Evaluation

Subject testing was performed at the Massachusetts Institute of Technology (MIT) Media Lab Biomechanics Gait Laboratory. Participants were informed of and consented to test protocols approved by the MIT Institutional Review Board: the Committee on the Use of Humans as Experimental Subjects. All subjects self-reported to be healthy with activity levels at or above K3, K4: having ambulatory activity with variable cadence. The Biomechanics Gait Lab facility includes a 15m walkway, a VICON motion capture system, and an instrumented split treadmill.

We aimed to verify the actuator’s ability to replicate biologically relevant torque and velocity capabilities by testing it on a human subject while configured as a foot-ankle powered prosthesis. The preliminary results include a 75kg male subject with unilateral below knee amputation walking on a treadmill at specified speeds. Experimental procedures included donning and adjustment of the TF8 to match the alignment and comfort of the participant’s standard issued prosthesis. Control parameters were then tuned to match the comfort level of the subject as they acclimated to walking at self-selected speed with the powered ankle-foot system. The parameters available to tune include virtual parallel stiffness, push-off torque threshold, push-off torque ramp rate, push-off stiffness, toe-off angle and damping. During the experiments, on-board sensors recorded and transmitted the full actuator state across a wireless bluetooth communication protocol to a secondary computer at a rate of 100Hz. Data collected included joint angle, velocity, torque, finite-state, as well as motor current and voltage.

III. RESULTS

A. Mechanical Design

1) *Structure*: The load path transmits joint torque as a force down the axis of the ballscrew, through the motor bearing stack, through the pivots to the moment arm. This moment arm then transfers the force primarily as a moment that is then grounded into the frame that supports the output joint axle. From the bolted interface at the frame, the load could be transmitted to any desired structure. For this prosthesis application, the load is transmitted through Aluminum 7075-T6 structural routing features to a standard lower extremity prosthesis pyramid interface such that it may be mounted to a socket. These elements were designed to allow a maximum transverse deflection of 3.4mm as specified by estimates of biological bone loading [26], [27] in addition to sustaining fatigue life estimates of a $0.3\sigma_u$ ultimate stress for aluminum.

Fig. 5(a,b) shows the load path through the structure and the load path through the motor bearing stack. Operation of the actuator under maximum spring deflection is also shown in Fig. 5(a). The dotted-line arrow is an applied joint torque, τ_l and the solid arrow is force from motor displacement along the length of the screw, F_s . The green dotted line in both Fig. 5(a)

and (b) shows the load path when the structure experiences compression loads. The motor bearings were replaced with angular contact bearings in order to support the axial load of the screw. The load paths through the angular contact bearings differ when experiencing compression and tension loads due to their high contact angle. The orange solid line in Fig. 5 (b) shows the circuitous tension load path from pivots, through the bearing stack inside the motor and through the ball-nut presser flange before passing into the ball-nut and ball-screw. These loads are physically mirrored to both pivots and distributed circumferentially throughout the projected areas.

The actuator architecture of TF8 could be called a moment-coupled cantilever-beam reaction-force series elastic actuator. The configuration shown in Fig. 1 shows the actuator assembled in an ankle embodiment. TF8 applies a torque to the joint by coupling a linear actuator to a moment arm a distance from the joint axis. The linear actuator is composed of an outrunner motor with integrated ballscrew to generate linear force. Reaction-force from this linear actuator induces a moment on the cantilever-beam spring by way of a moment arm clamped to the spring, creating a force-couple. The spring finally serially grounds the load to the frame of the actuator. Four bolts attach the spring enabling it to be swapped to match the actuator to its application, such as users of different mass and to match the dynamics of either an ankle or knee. Configured as an ankle the output joint placement is designed to match the relative orientation of the BiOM powered ankle [1] when mounted on an Össur Vari-flex foot [38] – the unloaded height of the ankle is 67mm and lateral placement with respect to mounting holes in the Vari-flex is matched. Matching alignment allows direct kinematic comparison to BiOM. The minimum working actuator configuration as shown in Fig. 5(a) has a mass of 1.36kg. The overall hardware mass as a knee, not including electronics or battery measures 1.6kg, and the breakdown of that mass distribution is shown in Table III. The electronics and wiring weigh 53g and 52 g, respectively. The battery used for walking experiments is composed of two 3S 11.1V 1.0Ah lithium polymer hobby-grade batteries connected in series for a nominal operating voltage of 22.2V; the battery combined mass is 180g and is usually located off-board on a user’s socket. The fully equipped actuator configured as shown in Figs. 1 and 6 with on-board electronics, flex-foot, adapters and battery together weigh 2.0kg.

The system specification achieved for the TF8 is a peak torque of 180Nm, a root mean square torque rating of 85Nm with a total range of motion of 115 degrees and a velocity of 6.0rad/s at the joint. The hardware mass of the knee, 1.6kg, is 65% of the weight of an equivalent leg segment for the target 90kg user. System heights are shown in Fig. 6: the height of the actuator from pyramid adapter mount to rotary output mount is 171mm, from mounting point to rotary joint is 156mm, and the overall unloaded *clearance* height with a Vari-flex foot is 223mm.

2) *Linkage Geometry*: The overall gear ratio is nominally $52 : 1 \pm 3.5$ during level ground walking. At high flexion the gear ratio can sweep as low as $2 : 1$ as the actuator approaches limits to its controlled range of motion. This

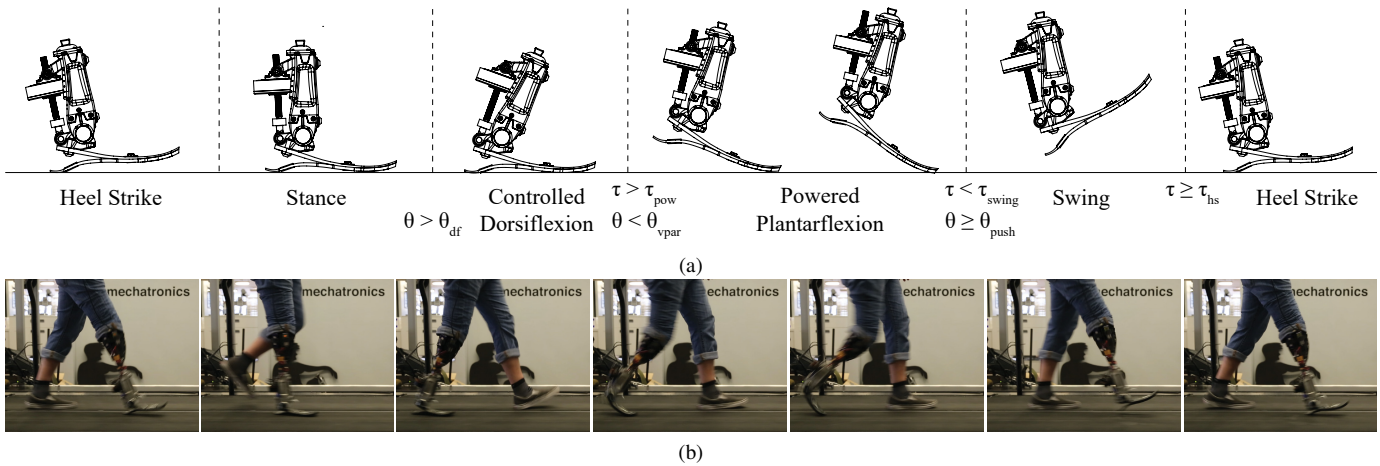


Fig. 4. Schematic and human subject demonstration of state transitions: (a) State transitions are triggered by torque and angle thresholds tuned to meet test subject preferences. (b) A subject walking with the finite-state machine controller. Note during powered plantarflexion the additional series elasticity contributed by the Variflex foot that is not accounted for in the numerical models.

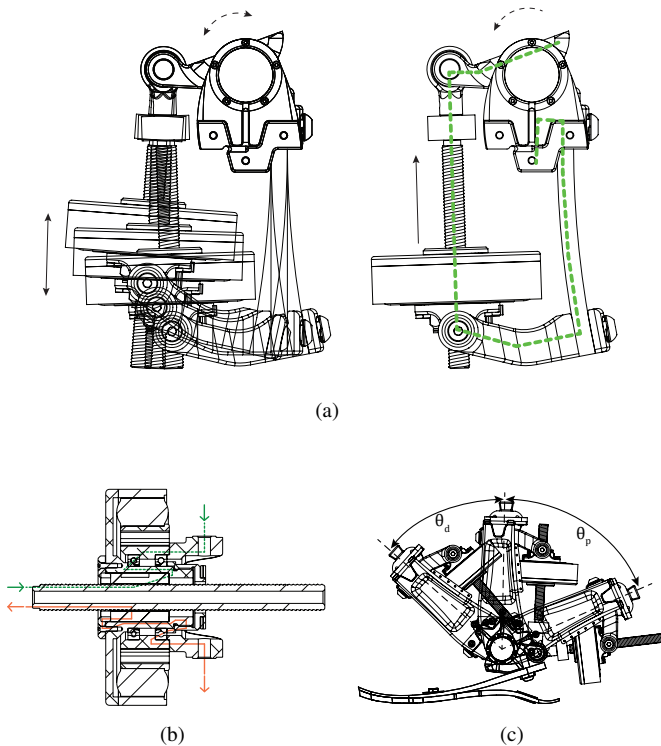


Fig. 5. (a) Spring deflection occurs when a torsional load (dotted arrow) is applied at the rotary output. Image on the right shows the load path from the applied load at the joint, through the linear actuator, the cantilever spring and to the structural frame. (b) The compression load-path is shown as the dotted line, while the tension load-path is shown as the solid line through the motor bearing stack. (c) The full range of motion of the ankle configured TF8 prosthesis.

motion is achieved with a Thomson Linear 5mm lead ball-screw (BSPRM012L05M) and nut (KGM-N-1205-RH) located a projected perpendicular distance nominally 41 mm from the joint axis. The ballscrew and motor are mounted in needle-bearing pivots at the motor base and the rotary output arm allowing angular alignment throughout the range of motion

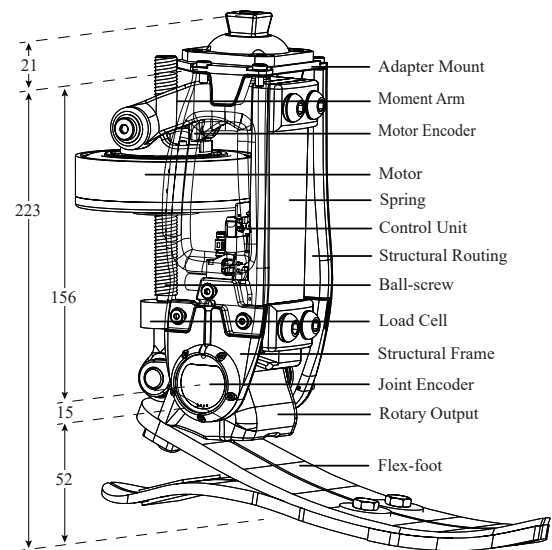


Fig. 6. The TF8 Actuator is shown configured as an ankle powered prosthesis with the components labeled and sizing. Actuator minimum build height is 171mm from mounting platforms..

TABLE III
MASS DISTRIBUTION OF THE TF8 KNEE ACTUATOR HARDWARE

Component	Mass (g)	(%)
Structural Components	556	35
Motor	549	34
Spring	116	7
Ballscrew	100	6
Spring Clamping Hardware	95	6
Load Cell	54	3
Fasteners	48	3
Pyramid Adapter	48	3
Encoder Hardware	45	2
Total	1592	100

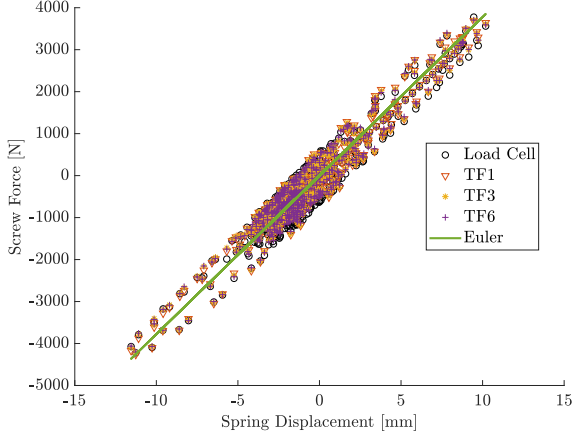


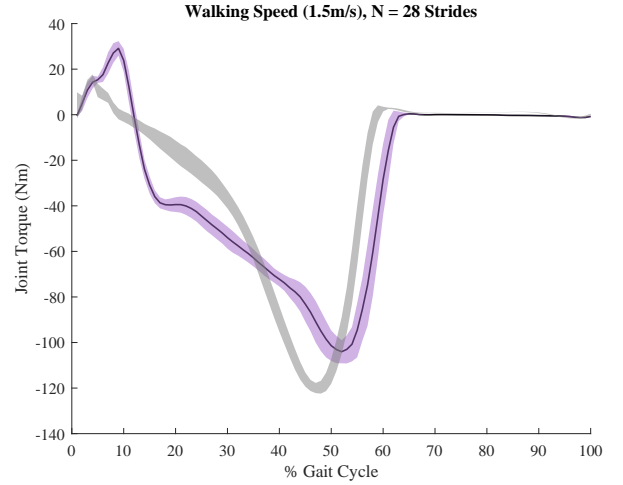
Fig. 7. A load cell in-line with the ball-screw measured real force in the screw. Shown here is the 12.4mm thick, 378kN/m fiberglass spring. (a) Transfer function estimates of axial force to spring linear displacement are shown as is a linearized model of an Euler-Bernoulli bending beam. The load cell measurements show hysteresis.

of the actuator. The total range of controllable motion is 115 degrees. Mechanically, the system can reach 120 degrees to enable the additional range of motion for passive tasks such as when used as a knee actuator and a user wishes to sit cross-legged.

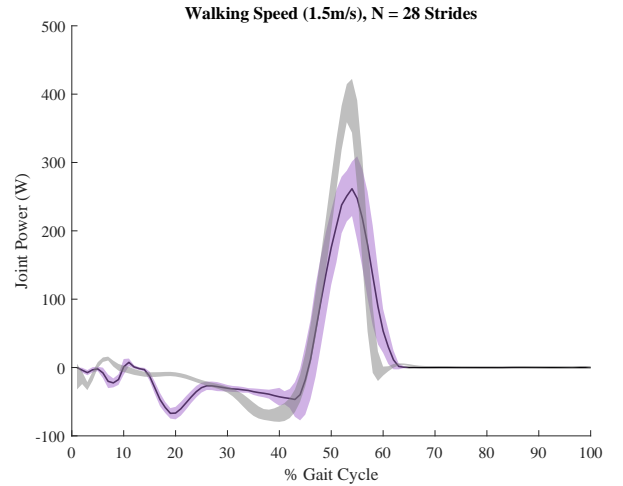
3) *Motor*: The motor is a frameless T-Motor U10 Plus KV100 outrunner motor [39] capable of producing instantaneous peak torque of 4 Nm and 3000 rpm at 24V bus voltage. We designed a custom rotor and stator to integrate the ball-nut directly into the rotor and to replace the motor bearings with high axial strength thin-section angular contact bearings. Axial pre-load comes from a nut that also retains a magnetic motor encoder rotor disk. The motor bearing stack and associated load path can be seen in Fig. 5b.

4) *Series Elastic Element*: Optimization defined a nominal series stiffness $K_s = 271 \frac{kNm}{m}$, a 8.6mm thick spring. However, after initial testing we included a heavier spring to accommodate an overall lower than expected structural stiffness. The configuration as built utilizes a 42 mm x 12.44 mm thickness beam with a sprung length of 86 mm and an overall measured linear stiffness of 378 kN/m Fig. 21. The maximum deflection is limited to 13mm linear translation by mechanical features built into the structure; at 13mm of deflection the spring experiences nearly 265Nm or torque and stores 19 Joules of mechanical energy. The spring is a unidirectional E-glass fiberglass composite (GC-67-UCB) manufactured by Gordon Composites [23].

Repeatable variation was visible in stiffness measurements. To accommodate the damped hysteresis behavior we mapped several transfer functions with differing pole/pair combinations and an Euler-Bernoulli beam. The results show variation of up to 5% so the Euler-Bernoulli 21 was fit and used for encoder-based force sensing.



(a)



(b)

Fig. 8. Preliminary results from one subject walking with the finite state-machine controller. The black line is the mean, purple shows one standard deviation, grey is one standard deviation of able-bodied walking data from [14].

B. Preliminary Clinical Evaluation

Torque and power from a 75kg person with unilateral below knee amputation walking with a finite-state machine controller on a treadmill at 1.5 m/s is shown in Fig. 8. Twenty-eight strides were acquired and aligned on a percent gait cycle plot. The ankle joint mean torque shows a slight phase-lag and undershoot of mean data, though does achieve about 108Nm at powered push-off. Mechanical power aligns well with mean data, but again the 250 W measured at the joint undershoots biological of 380W, for a 75kg subject.

IV. DISCUSSION

A. Mechanical Design

This cantilever-beam reaction-force series elastic configuration enables convenient and mass efficient mechanical packaging. The moment-couple produces uniform strain along the length of the beam, thus maximizing material utilization

while minimizing mass. This spring arrangement allows a build height reduction by wrapping the spring back along the length of the linear actuator, rather than a traditional SEA arrangement of coil springs stacked serially along the linear actuator axis [40]. Traditional SEA configurations often rely on secondary linear bearings to support motion of the intermediary coupling between spring, motor and output. In this case, the spring acts as a flexure to support displacements of both the spring and motor. This design improves upon the leaf-spring configuration [41] used, by replacing the universal joint constraints with the flexure behavior of the spring in addition to allowing axial play with spring washers in the perpendicularly arranged pivots to manage manufacturing misalignments. Further differentiation is removal of the commonly used intermediary belt-drive gear reduction by using a large gap-radius motor with relatively high torque. Implementing the torque-motor in a frameless configuration reduces the redundant mass often required to serially couple the screw and nut to the motor. Combining a ball-nut with an outrunner motor rotor and the use of a yoke pivot is similar to [18] but rather than serially stacked discrete components, our new design integrates the nut directly into the rotor and the supporting yoke directly into the stator support. This integration allows the ball-screw to pass entirely through motor, increasing range of motion while decreasing build height.

The relatively high-torque of the U10 motor allows a smaller gear reduction than the smaller diameter Maxon EC-4 Pole inner rotor motor commonly used in other published hardware [9], [20], [34]. Reflected inertia is a critical parameter in both control bandwidth as well as user safety in high impedance contact conditions. Larger radius motors have an r^2 inertia increase yet are not subject to as large of a N^2 drivetrain reflected inertia contribution. The trade-offs between reflected inertia of rotor and drivetrain tends to nullify one another [42]. Since reduced gearing generally benefits drive-train efficiency larger torque motors with lower reductions tend to have slightly improved performance.

A secondary user experience driver towards larger torque motors is that smaller diameter motors operate at higher rpm, generating higher frequency audible noise. Removing this high frequency element can reduce the audible noise range to a more qualitatively pleasing frequency range.

The larger inertia of the outrunner motor does, however, have a drawback related to its larger inertia. The reaction torque from high acceleration motions can propagate through the structural chain and to the user. This motor can generate up to 3.5Nm of torque in normal operation, and while that reaction torque was initially considered in the loading on the spring, its effect on the user was not realized until parts were already under manufacture. The solution to this problem is smooth trajectory generation with minimum jerk to minimize the reaction yaw torque on the user.

The reaction-force coupled moment cantilever beam spring excels in a few ways and has one drawback discussed below. The flat plate beam can be routed back along the length of the linear actuator, reducing overall system height when compared to helical springs. The cantilever beam also acts as a precision flexural element providing its own translational constraint

negating the need for additional bearings or guideways to constrain deflection motions. Finally, manufacturing of a flat plate cantilever beam is relatively straightforward, enabling multitudes of springs to be available to tune performance to different users or applications. The TF8 design enables static reconfiguration: by releasing four bolts the spring can be swapped for a another to match user mass and application. This functionality is similar to [43] but with a simpler attachment means and without adjusting the cantilever length. Construction of the plate from fiber composite structures also enables aligning unidirectional tensile fibers, exploiting the primary benefit of composite structures – enabling composites to far out perform metallic alternatives for energy density, as shown in Table II.

There are two unfortunate conditions that occur with the load path configuration of this actuator: the first is inherent to the reaction-force configuration and the second could be mitigated with a second design iteration. The actuator remains fully controllable even with both design flaws however they do show up as small nonlinearities in operation. The *reaction force* spring configuration creates a relatively large sprung mass of the motor, moment arm and spring. The motion trace image in Fig. 5(a) demonstrates the behavior of the motor mass motion.

The additional reflected sprung mass of the motor in addition to rotor inertia during high impedance motions reduces system natural frequency making control potentially difficult near that frequency. This behavior is evident when the user lightly loads the toe and brings the foot-spring into play in a middle inertia condition. The SEA is evaluated in a high impedance condition (stance), and in low-impedance (swing), but we generally do not evaluate this condition where the overall system stiffness is affected by the additional series spring of a flex-foot. In this case system natural frequency is lowered by low stiffness and the larger mass of the weight of a leg - a behavior that is evident biologically too, when ones leg is partially suspended on a toe. This is an area open to further investigation.

During numerical simulation we underestimated the natural frequency of the actuator; where we set out upon a design for a 13 Hz natural frequency actuator we instead designed for a 2.2 Hz natural frequency actuator by not including structural stiffness with the designed series spring stiffness. This has so far proven adequate for experiments with multiple subjects walking on the ankle, but potentially poses some complications for high performance control. The second issue in the design can also be seen in Fig. 5: the ballnut resides an offset distance from the motor support pivot. This offset allows a moment to be applied to the ballnut under heavy compression loading - likely limiting the lifetime of the ball-nut due to the geometry of the internal ball returns. In tension the configuration remains naturally stable, but in compression there is instability about the pivot. This pivot condition shows up as backlash around the zero load condition where there is some small play in how the motor and ball-nut seat against the screw.

Regarding system electrical energy: there is limited energetic opportunity during controlled dorsiflexion, though a negative work phase of gait, the low velocity limits the energy

transfer to the motor while most of the energy is stored in the spring – this is evident in the spring displacement curves. The majority of the power flow occurs at the transition from late-stance push-off to early-swing when the motor must actually accelerate out of its way to allow the toe return. The limited energetic cost of controlled dorsiflexion does lay to question the focus on parallel springs in ankles from an energetics point of view. The trade-off of the parallel spring is that of kinetic, kinematic and design complexity costs. For our efforts to build a hardware research platform we leaned into enabling larger range of motion and rely on the actuator power electronics and control to generate proper kinetics.

B. Preliminary Walking Results

Walking with a finite-state machine shows the actuator generally tracks biological kinetics and kinematics but has room for improvement. The joint torque shows some phase lag and undershoot compared to mean biological data. The discrepancy in torque and power may be due to both differences in the estimation of a finite-state machine and biological waveform, as well as potentially limited torque tracking capability of our low-level torque controller.

The state-machine settings and transition parameters were tuned to user comfort, but this does not necessarily align with biology. One hypothesis is that because amputee subjects are often accustomed to stiff, passive or joint limited powered ankle joints, some people find large ankle range of motion unsettling or even unstable. Though data from one user is shown in this study, we have had nine subjects wear the device during initial testing. A non-scientific evaluation of preference seems to suggest people with more recent amputation have tend towards a softer, larger range of motion ankle virtual springs. The user in this study had preference for a stiff ankle joint, limiting range of motion.

The torque control was manually tuned by hand, leaving room for improved performance with the inclusion of feed-forward control, friction compensation, and more sophisticated lead-lag control than manual tuned PID. This hardware is a platform on which future development in these areas can expand performance capabilities.

V. CONCLUSIONS

The TF8 actuator is one of the lightest weight, most powerful bionic knee and ankle platforms, and it shows promise of enabling high-activity-level performance. We have shown it is capable of producing 175 Nm of torque, biological ranges of power and has a mass of 1.6 kg - one of the lighter weight research-level powered prostheses. By integrating the ball-nut directly into the motor rotor and utilizing the spring as both energy storage and motion constraint we were able to reduce the design complexity and build the actuator into a standalone actuation unit. The TF8 actuator could potentially be used for other humanoid, quadruped or robotic applications by replacing the structural elements with a designer's application specific hardware and desired springs.

The system is not without design flaws though: the nominal design natural frequency is lower than initially expected and

there are nonlinearities around zero load due to backlash in the ball-nut and its arrangement with respect to the motor support pivot. Neither of these design issues have proven a problem in initial testing with subjects and manually tuned PID torque control.

The process of searching for a minimum electric energy consumption per gait cycle configuration of design components proved effective at identifying a hardware specification. Discrete availability of hardware limits the ability to smoothly search across the space and thus forces additional compromise in the design. Further, the kinematic clamped analysis is a good starting point however we would recommend future design attempts to utilize a more sophisticated actuator model that includes controller effort. The process of disqualifying designs based on behavior that fails search constraints may be limiting when controller effort could allow generally better agreed behavior across the wider trajectory with torque, velocity or motor current and voltage saturation at only a few data points. Further, inclusion of a dynamic system model with control effort could potentially give better understanding of final system response.

Finally, in the design of TF8 we attempted to not only build a high performance, cost-effective actuator capable of performing multiple functionalities, we also strove to include aesthetic in the design of our hardware. At the end of the day we are building hardware to replace the function of lost body-parts. The people who have the opportunity to make use of our hardware should be inspired not only by the technology but by our effort to push the limits of how disability is perceived.

AUTHOR CONTRIBUTIONS

Matt Carney performed all analyses, designed and built the hardware, programmed the controls, and ran the experiments. Tony Shu made substantial contributions to the code base, Roman Stolyarov helped with establishing the finite-state machine transitions and code base and Jean-Francois Duval built the FlexSEA embedded system. Hugh Herr is the Director of the MIT Media Lab Biomechatronics Group.

ACKNOWLEDGMENT

The authors would also like to thank our brave test-pilots and the machine shops who helped produce great hardware: Production Robotics in California, MIT Central Machine Shop, Mark Belanger at MIT Edgerton Student Shop, Gordon Composites, and in China: Star Rapid and T-Motor. Special thanks to Jean-Francois Duval from Dephy, Inc. who worked closely with Matt to customize the FlexSEA system for this application. Finally, the authors thank our funding sources for enabling this research, and our colleagues in the field contributing to the greater knowledge.

REFERENCES

- [1] Bionx, "The BiOM Advantage - BionX Medical Technologies," 2017.
- [2] Össur, "Össur Dynamic Solutions Power Knee™," 2018.
- [3] G. A. Pratt and M. M. Williamson, "United States Patent (19) 11 Patent Number : Date of Patent ;," 1995.
- [4] S. K. Au, J. Weber, and H. Herr, "Biomechanical Design of a Powered Ankle-Foot Prosthesis," in *IEEE 10th International Conference on Rehabilitation Robotics*, 2007, pp. 298–303.

- [5] P. Cherelle, V. Grosu, A. Matthys, B. Vanderborght, and D. Lefeber, "Design and validation of the ankle mimicking prosthetic (AMP-) Foot 2.0," *IEEE Transactions on Neural Systems and Rehabilitation Engineering*, vol. 22, no. 1, pp. 138–148, 2014.
- [6] P. Cherelle, V. Grosu, M. Cestari, B. Vanderborght, and D. Lefeber, "The AMP-Foot 3, new generation propulsive prosthetic feet with explosive motion characteristics: Design and validation," *BioMedical Engineering Online*, vol. 15, no. 3, pp. 21–36, 2016.
- [7] R. D. Bellman, M. A. Holgate, and T. G. Sugar, "SPARKy 3: Design of an active robotic ankle prosthesis with two actuated degrees of freedom using regenerative kinetics," *Proceedings of the 2nd Biennial IEEE/RAS-EMBS International Conference on Biomedical Robotics and Biomechatronics, BioRob 2008*, pp. 511–516, 2008.
- [8] M. A. Holgate, J. K. Hitt, R. D. Bellman, T. G. Sugar, and K. W. Hollander, "The SPARKy (spring ankle with regenerative kinetics) project: Choosing a DC motor based actuation method," *Proceedings of the 2nd Biennial IEEE/RAS-EMBS International Conference on Biomedical Robotics and Biomechatronics, BioRob 2008*, pp. 163–168, 2008.
- [9] M. Grimmer, M. Holgate, J. Ward, and A. Boehler, "Feasibility study of transtibial amputee walking using a powered prosthetic foot," in *International Conference on Rehabilitation Robotics (ICORR)*, 2017, pp. 1118–1123.
- [10] Ottobock, "C-Leg 4: Microprocessor Knee — Ottobock UK," 2018.
- [11] A. D. Kuo, "A simple model of bipedal walking predicts the preferred speed-step length relationship," *Journal of biomechanical engineering*, vol. 123, no. 3, pp. 264–269, 2001.
- [12] A. Protopapadaki, W. I. Drechsler, M. C. Cramp, F. J. Coutts, and O. M. Scott, "Hip, knee, ankle kinematics and kinetics during stair ascent and descent in healthy young individuals," *Clinical Biomechanics*, vol. 22, no. 2, pp. 203–210, 2007.
- [13] M. E. Carney and H. M. Herr, "Energetic Consequences of Series and Parallel Springs in Lower-Extremity Powered Prostheses," *EngrXiv*, DOI: 10.31224/osf.io/swt34, 2019.
- [14] J. Markowitz, "A Data-Driven Neuromuscular Model of Walking and its Application to Prosthesis Control," Ph.D. dissertation, Massachusetts Institute of Technology, 2013.
- [15] D. S. Pieringer, M. Grimmer, M. F. Russold, and R. Rienen, "Review of the actuators of active knee prostheses and their target design outputs for activities of daily living," *2017 International Conference on Rehabilitation Robotics (ICORR)*, pp. 1246–1253, 2017.
- [16] C. E. Clauser, J. T. McConville, and J. W. Young, "Weight, Volume, and Center of Mass of Segments of the Human Body," *National Technical Information Service*, pp. 1–112, 1969.
- [17] T. Verstraten, J. Geeroms, G. Mathijssen, B. Convens, B. Vanderborght, and D. Lefeber, "Optimizing the power and energy consumption of powered prosthetic ankles with series and parallel elasticity," *Mechanism and Machine Theory*, vol. 116, pp. 419–432, 2017.
- [18] S. Wang, C. Meijneke, and H. van der Kooij, "Modeling, design, and optimization of Mindwalker series elastic joint," jun 2013, pp. 1–8.
- [19] E. J. Rouse, L. M. Mooney, and H. M. Herr, "Clutchable series-elastic actuator: Implications for prosthetic knee design," *The International Journal of Robotics Research*, vol. 33, no. 13, pp. 1–15, nov 2014.
- [20] J. Zhu, H. She, and Q. Huang, "PANTOE II: Improved Version of a Powered Transtibial Prosthesis With Ankle and Toe Joints," in *Proceedings of the 2018 Design of Medical Devices Conference*. Minneapolis, MN, USA: ASME, 2018, pp. 1–3.
- [21] D. Paluska and H. Herr, "The effect of series elasticity on actuator power and work output: Implications for robotic and prosthetic joint design," *Robotics and Autonomous Systems*, vol. 54, pp. 667–673, 2006.
- [22] A. M. Wahl, *Mechanical Springs*, 2nd ed. Cleveland, Ohio: Penton Publishing Company, 1949.
- [23] Gordon Composites, "GC-67-UB," Gordon Composites, Montrose, Colorado, Tech. Rep., 2017.
- [24] D. E. Galloway, Kevin C and Clark, Jonathan E and Koditschek, "Design of a tunable stiffness composite leg for dynamic locomotion," *ASME 2009 International Design Engineering Technical Conferences and Computers and Information in Engineering Conference*, no. August, pp. 215–222, 2009.
- [25] Futek, "LCM 300 Axial Load Cell," Futek, Tech. Rep., 2011.
- [26] C. Milgrom, M. Gildadi, A. Simkin, N. Rand, R. Kedem, H. Kashtan, M. Stein, and M. Gomori, "The area moment of inertia of the tibia: A risk factor for stress fractures," *Journal of Biomechanics*, vol. 22, no. 11-12, pp. 1243–1248, 1989.
- [27] P. F. Yang, M. Sanno, B. Ganse, T. Koy, G. P. Brüggemann, L. P. Müller, and J. Rittweger, "Torsion and antero-posterior bending in the in vivo human tibia loading regimes during walking and running," *PLoS ONE*, vol. 9, no. 4, 2014.
- [28] X. Wang, J. Nyman, X. Dong, and H. Lench, *Fundamental Biomechanics in Bone Tissue Engineering*. Morgan & Claypool Publishers, 2010.
- [29] R. J. Minns, J. Campbell, and G. R. Bremble, "The bending stiffness of the human tibia," *Calcified Tissue Research*, vol. 17, no. 2, pp. 165–168, 1975.
- [30] J. F. Duval and H. M. Herr, "FlexSEA: Flexible, Scalable Electronics Architecture for wearable robotic applications," *Proceedings of the IEEE RAS and EMBS International Conference on Biomedical Robotics and Biomechatronics*, vol. 2016-July, pp. 1236–1241, 2016.
- [31] N. Paine, S. Oh, and L. Sentis, "Design and Control Considerations for High-Performance Series Elastic Actuators," *IEEE/ASME Transactions on Mechatronics*, vol. 19, no. 3, pp. 1080–1091, jun 2014.
- [32] V. L. Orekhov, C. S. Knabe, M. A. Hopkins, and D. W. Hong, "An un lumped model for linear series elastic actuators with ball screw drives," in *International Conference on Intelligent Robots and Automation*. IEEE, 2015, pp. 2224–2230.
- [33] J. Sup, A. Bohara, and M. Goldfarb, "Design and Control of a Powered Knee and Ankle Prosthesis," in *IEEE 10th International Conference on Rehabilitation Robotics*. Noordwijk, The Netherlands: IEEE, 2007, pp. 4134–4139.
- [34] S. K. Au and H. M. Herr, "Powered Ankle-Foot Prosthesis," *IEEE Robotics & Automation Magazine*, no. September, pp. 52–59, 2008.
- [35] M. Goldfarb et al., "Realizing the promise of robotic leg prostheses," *Science translational medicine*, vol. 5, no. 210, p. 210ps15, nov 2013.
- [36] B. E. Lawson, J. Mitchell, D. Truex, A. Shultz, E. Ledoux, and M. Goldfarb, "A robotic leg prosthesis: Design, control, and implementation," *IEEE Robotics and Automation Magazine*, vol. 21, no. 4, pp. 70–81, 2014.
- [37] A. H. Shultz, B. E. Lawson, and M. Goldfarb, "Running with a powered knee and ankle prosthesis," *IEEE Transactions on Neural Systems and Rehabilitation Engineering*, vol. 23, no. 3, pp. 403–412, 2015.
- [38] Össur, "Vari-Flex," Össur, Tech. Rep., 2019.
- [39] T-Motor, "T-Motor," 2017.
- [40] D. W. Robinson, J. E. Pratt, D. J. Paluska, and G. A. Pratt, "Series elastic actuator development for a biomimetic walking robot," in *International Conference on Advanced Intelligent Mechatronics*. Atlanta: IEEE/ASME, 1999, pp. 561–568.
- [41] C. Knabe, B. Lee, V. Orekhov, and D. Hong, "Design of a Compact, Lightweight, Electromechanical Linear Series Elastic Actuator," in *ASME International Design Engineering Technical Conferences and Computers and Information in Engineering Conference, Volume 5B: 38th Mechanisms and Robotics Conference*. Buffalo, NY: ASME, 2014, pp. 1–8.
- [42] A. Wang, S. Seok, A. Wang, D. Otten, and S. Kim, "Actuator Design for High Force Proprioceptive Control in Fast Legged Locomotion Actuator Design for High Force Proprioceptive Control in Fast Legged Locomotion," in *IEEE/RSJ International Conference on Intelligent Robots and Systems*, no. October. Vilamoura: IEEE, 2012, pp. 1970–1975.
- [43] V. Orekhov, D. Lahr, B. Lee, and D. Hong, "Configurable Compliance for Series Elastic Actuators," in *ASME International Design Engineering Technical Conferences and Computers and Information in Engineering Conference, Volume 6B: 37th Mechanisms and Robotics Conference*. Portland, Oregon: ASME, 2013, pp. 1–8.